A Bi-Lineage Conducive Scaffold for Osteochondral Defect Regeneration

Yan Wu, Shouan Zhu, Chengtie Wu, Ping Lu, Changchang Hu, Si Xiong, Jiang Chang, Boon Chin Heng, Yin Xiao, and Hong Wei Ouyang**

Because cartilage and bone tissues have different lineage-specific biological properties, it is challenging to fabricate a single type of scaffold that can biologically fulfill the requirements for regeneration of these two lineages simultaneously within osteochondral defects. To overcome this challenge, a lithium-containing mesoporous bioglass (Li-MBG) scaffold is developed. The efficacy and mechanism of Li-MBG for regeneration of osteochondral defects are systematically investigated. Histological and micro-CT results show that Li-MBG scaffolds significantly enhance the regeneration of subchondral bone and hyaline cartilage-like tissues as compared to pure MBG scaffolds, upon implantation in rabbit osteochondral defects for 8 and 16 weeks. Further investigation demonstrates that the released Li+ ions from the Li-MBG scaffolds may play a key role in stimulating the regeneration of osteochondral defects. The corresponding mechanistic pathways involve Li+ ions enhancing the proliferation and osteogenic differentiation of bone mesenchymal stem cells (BMSCs) through activation of the Wnt signalling pathway, as well as Li+ ions protecting chondrocytes and cartilage tissues from the inflammatory osteoarthritis (OA) environment through activation of autophagy. These findings suggest that the incorporation of Li+ ions into bioactive MBG scaffolds is a viable strategy for fabricating bi-lineage conducive scaffolds that enhance regeneration of osteochondral defects.

1. Introduction

It is well known that osteoarthritis is a major healthcare challenge worldwide.[1] Two major pathological characteristics of osteoarthritis are the degradation of articular hyaline cartilage and structural remodeling of subchondral bone.[2] Tissue engineering based strategies, in particular microfracturing and autologous chondrocyte implantation (ACI)-technique, have been demonstrated to be effective treatment modalities for the regeneration of joint surface cartilage.[3,4] Osteochondral defect repair is much more challenging as it requires the simultaneous restoration of both cartilage and bone tissue.[5] Since cartilage and bone tissues have different lineage-specific biological properties, it is challenging to utilize a single type of scaffold to biologically fulfill the disparate requirements for regenerating these two lineages in osteochondral defects.

Previous studies have shown that subchondral bone plays a key role in OA onset and progression.[6] Cao et al. reported that activation of TGF-β in subchondral bone initiated pathological changes associated with osteoarthritis.[7,8] Our previous study showed that the implantation of bioactive materials in subchondral bone defects supported the preservation of autologous cartilage.[9] Various types of scaffolds, including stratified and non-stratified scaffolds, have been developed for repair and regeneration of subchondral defects.[10] To repair subchondral defects, the simultaneous regeneration of both cartilage and bone tissues is of

Y. Wu, S. Zhu, P. Lu, C. Hu, S. Xiong,
Prof. H. W. Ouyang
Center for Stem Cell and Tissue Engineering
School of Medicine
Zhejiang Provincial Key Lab for Tissue Engineering and Regenerative Medicine
Zhejiang University
866 Yu Hang Tang Road
Hangzhou 310058, China
E-mail: hwoy@zju.edu.cn

Prof. C. Wu, J. Chang
State Key Laboratory of High Performance Ceramics and Superfine Microstructure
Shanghai Institute of Ceramics
Chinese Academy of Sciences, 1295 Dingxi Road
Shanghai 200050, China
E-mail: chengtiewu@mail.sic.ac.cn

B. C. Heng
Department of Biosystems Science & Engineering (D-BSSE)
ETH-Zurich, Mattenstrasse 26
Basel 4058, Switzerland

Y. Xiao
Institute of Health and Biomedical Innovation
Queensland University of Technology
60 Musk Ave, Kelvin Grove
Brisbane, Queensland 4059, Australia

DOI: 10.1002/adfm.201304304

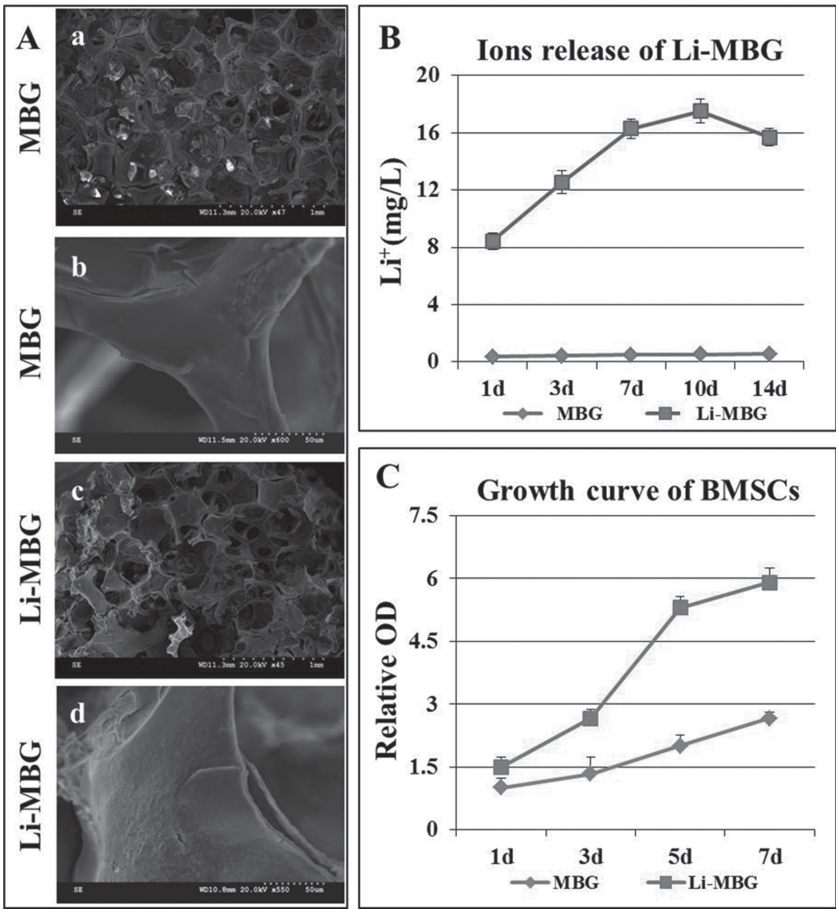

Figure 1. The microstructural and biological properties of Li-MBG scaffolds. (A) SEM images of MBG (a, b) and Li-MBG (c, d) scaffolds. (b, d) are at high magnification. Scale bars, 1mm (a, c), 0.05mm (b, d). (B) Profile of Li^+ ion release from Li-MBG scaffolds in DMEM. (C) The growth profile of BMSCs on MBG scaffold and Li-MBG scaffold.

great importance. Scaffolds can only be used for reconstructing either osseous tissues or chondral tissues, thus limiting their application for regeneration of osteochondral defects. Although two-layer scaffolds have been used for mimicking the macroscopic structure of cartilage and subchondral bone, it is difficult for these to biologically mimic the natural structure and function of cartilage and subchondral bone since the interface microstructure between cartilage and subchondral bone is quite complex.[11,12] Additionally, the bonding strength of fabricated two-layer scaffolds is often inadequate, which could result in delamination of the two layers of the scaffolds. To our knowledge, there are currently no smart scaffolds that exert bi-lineage functionality for preserving hyaline-like cartilage and regenerating mineralized bony tissues simultaneously.

Lithium (Li) has been widely used as a long-term mood stabilizer in the treatment of bipolar and depressive disorders for 50 years. Recently, oral administration of Li^+ ions was reported to enhance subchondral bone formation via activation of the canonical Wnt signaling pathway.[13,14] It was also reported that Li^+ ions could stimulate the osteogenic differentiation of BMSCs through activation of the canonical Wnt signaling pathway in vitro.[15] It is plausible that Li^+ ions can reverse aberrant activity and depletion of BMSCs reservoirs in subchondral bone, which are associated with degenerative changes in the joint.[16] Other studies showed that Li^+ exert its neuroprotective effects by increasing autophagy.[17,18]

Osteoarthritis (OA) is a degenerative as well as inflammatory disease of skeletal joints. In animal OA models, the low level of autophagy is associated with inflammatory stimulus as well as increased cell death and degradation in articular cartilage.[19] Both in vivo animal and clinical studies have demonstrated the key role of inflammation in OA pathogenesis.[20,21] The inflammatory cytokines, such as IL-1β, IL-6, and TNF-α, are now known to be deeply involved in OA progression.[22,23] It is likely that the intra-articular inflammatory environment inhibits successful cartilage regeneration with cell transplantation and scaffold implantation strategies. Based on the available scientific data, we hypothesize that Li^+ ions can protect cartilage by increasing the level of autophagy. Therefore, previous studies suggest that $Li^{\pm}$ ions may biologically fulfill the disparate requirements for dual-lineage (bone and cartilage) regeneration in osteochondral defects.

It is well-known that a conducive scaffold microenvironment is of great importance in tissue regeneration. Our previous studies have shown that a new kind of bioactive glass with well-ordered mesoporous structure, named as mesoporous bioglass (MBG), is a promising scaffold material for bone regeneration due to their excellent bioactivity.[24–31] MBG scaffolds possess highly inter-connective large pores (300–500 μm) that are similar to the porous structure of subchondral bone. Additionally, the well-ordered mesoporous channel structure (5 nm) improved bioactivity. Therefore, MBG scaffolds may be utilized for regeneration of subchondral bone due to their excellent bioactivity. Considering the possibility of bi-functional effects of Li^+ ions on both cartilage preservation and mineralized bony tissue regeneration, it would be of interest to design a Li-containing MBG (Li-MBG) scaffold for regeneration of osteochondral defects. Therefore, in this study, we aimed to develop a smart MBG scaffold with sustained Li^+ ion release. Additionally, the efficacy and underlying mechanism by which such a scaffold promote regeneration of osteochondral defects, will be investigated with both in vitro cell culture and in vivo animal-based osteoarthritis models.

2. Results

2.1. Physical and Biological Characterization of Porous Li-MBG Scaffolds

SEM analysis revealed that both Li-MBG and pure MBG scaffolds had a highly inter-connective porous structure

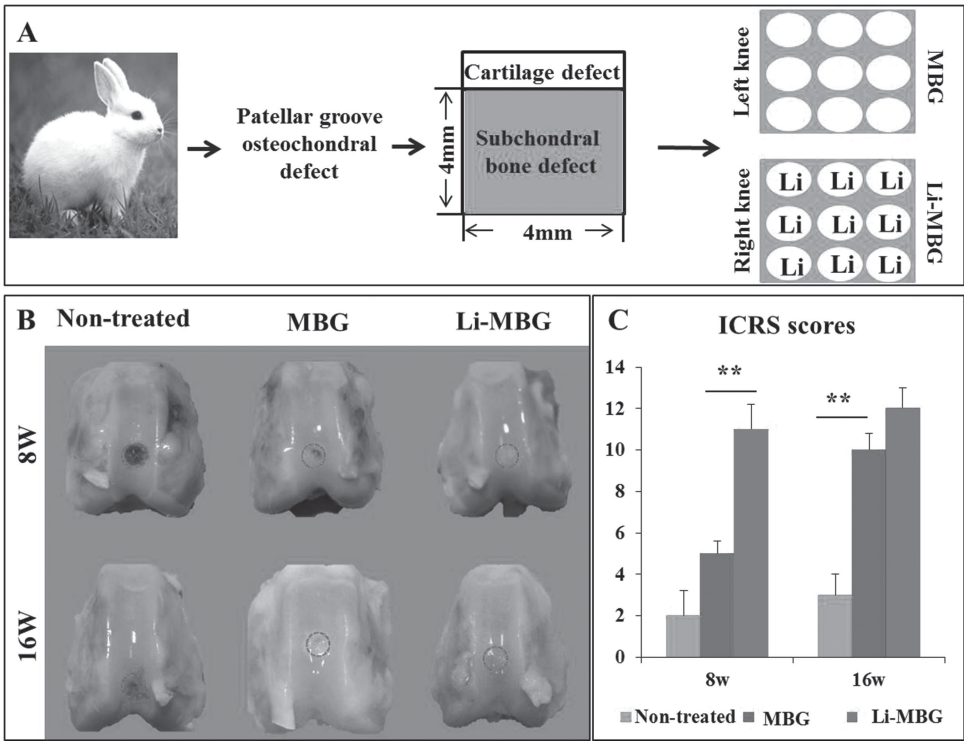

Figure 2. Macrophotographic comparison of the defects in the three experimental groups at 8 and 16 weeks post-surgery. A) Schematic representation of the experimental design. B) Macrophotographs showing the defects in the three experimental groups at 8 weeks (upper panels) and 16 weeks (lower panels) post-surgery. Knees were divided into non-treated group, MBG group and Li-MBG group. C) ICRS scores of non-treated group, MBG group, and Li-MBG group at 8 and 16 weeks post-surgery. Values are presented as mean ± standard deviation. ICRS, International Cartilage Repair Society.

and controllable pore size ranging from 300 to 500 μm (**Figure 1**Aa,c). Higher magnification images showed smooth surface of pore walls and no significant differences in the microstructure of the two scaffolds types (Figure 1Ab,d). The release profile of Li^+ ions from the Li-MBG scaffold system is shown in Figure 1B. There were no Li^+ ions released from MBG scaffolds, while there was sustained release of Li^+ ions from Li-MBG scaffolds with an increase of soaking time. Cell proliferation analysis by CCK-8 assay showed that BMSCs had a much higher proliferation rate on Li-MBG scaffolds than on pure MBG scaffolds (Figure 1C). These results illustrated that MBG based scaffolds possess appropriate physical and biological properties for cells adhesion and proliferation.

2.2. Efficacy of Li-MBG Scaffold for Osteochondral Defect Repair in a Rabbit Model

MBG based scaffolds were evaluated for osteochondral defect repair. At 8 and 16 weeks post-implantation, whole joints were collected for gross observation and histological analysis (**Figure 2**A). No distinct abrasion on the opposing articulating surface and no inflammatory reaction were observed at both 8 and 16 weeks post-implantation. There was no neo-tissue to be found in the non-treated group. Defects in the pure MBG group were filled with diseased and friable tissue while glossy white and well-integrated tissue was found in the Li-MBG group (Figure 2B). According to the ICRS scores from macroscopic observation, the average scores in the Li-MBG group were significantly higher than that of the non-treated and pure MBG groups at both 8 and 16 weeks post-implantation (Figure 2C). Micro-CT scans of the defect regions at 8 and 16 weeks demonstrated much more calcified tissue can be observed in the defect regions implanted with the Li-MBG scaffold at both the 8 and 16 weeks time points (Supporting Information Figure S1). These data exhibited that Li-MBG promoted the repair of bone tissue and cartilage tissues at the osteochondral defect.

2.3. Mechanism of Li-MBG Scaffold in Promoting Bone Regeneration

The mechanism of Li-MBG in promoting subchondral bone regeneration was investigated with BMSC culture model. CCK-8 analysis showed that proliferation of BMSCs at the low concentration range of Li^+ ions (lower or at 5 mM) had a measurable rate of increase over time, whereas cell proliferation was inhibited at higher concentrations of Li^+ ions (10 and 15 mM) (**Figure 3**A). We further evaluated the effect of Li^+ ions on osteogenesis of BMSCs, which was visualized by Alizarin Red Staining and quantified by optical density (OD) measurement at 405 nm. It was found that 5 mM of Li^+ ions significantly enhanced the osteogenic differentiation of BMSCs compared to the control group without Li^+ ions (Figure 3B). The OD value at a concentration of 5 mM Li^+ ions was markedly increased 1.2-fold ($P < 0.05$), as compared to that of the control group without

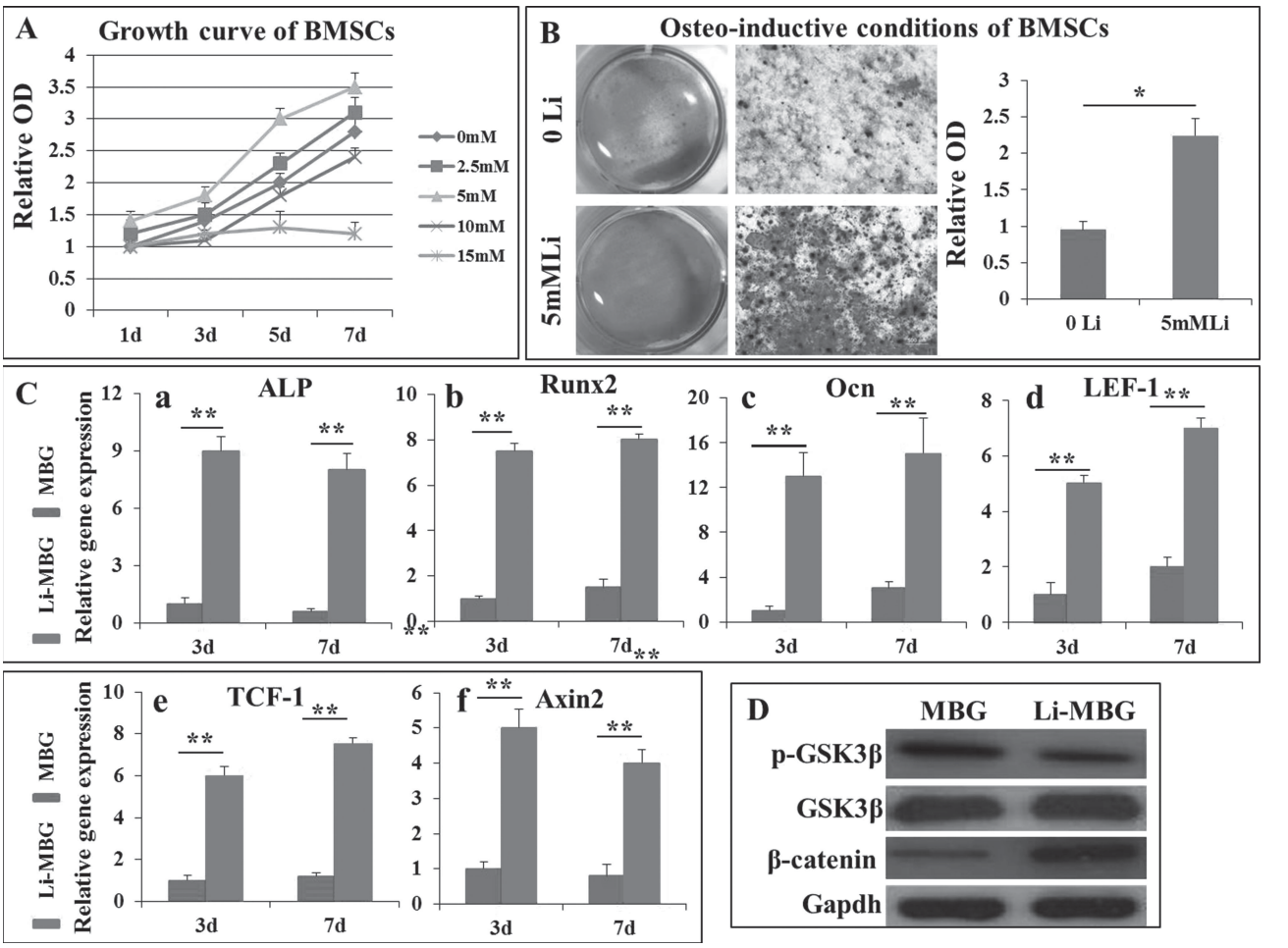

Figure 3. The effects of Li^+ ions on osteogenesis of BMSCs and the Wnt signaling pathway. A) BMSCs proliferation at a range of Li^+ concentrations. B) The effect of Li^+ ions on osteogenic differentiation of BMSCs visualized by Alizarin Red staining. C) The expression of bone-related genes (ALP, Runx2, and Ocn) and Wnt signaling pathway-related genes (LEF-1, TCF-1 and Axin2) by BMSCs cultured on MBG and Li-MBG scaffolds. D) β-catenin and p-GSK3β protein expression levels of BMSCs cultured on MBG and Li-MBG scaffolds were assessed by Western blot. * $P < 0.05$, ** $P < 0.01$.

Li^+ ions. Taken together, our results suggest that Li^+ ions at a concentration of 5 mM promoted proliferation and osteogenic differentiation of BMSCs.

To examine the synergistic effect of Li-MBG scaffolds on osteogenic differentiation of BMSCs, we analyzed gene expression of BMSCs in the osteogenic induction culture. The expression of ALP, Runx2 and Ocn genes by BMSCs on Li-MBG scaffolds were significantly upregulated on both day 3 and 7, as compared to the pure MBG scaffold group at corresponding time points (Figure 3Ca,b,c). To investigate the underlying mechanisms by which the scaffolds promoted osteogenic differentiation of BMSCs, we examined the canonical Wnt/β-catenin signaling pathway. RT-qPCR results showed a significantly increased expression of Wnt-related genes LEF-1, TCF-1, and Axin2 in the Li-MBG group compared to the MBG group on both day 3 and 7 (Figure 3Cd,e,f). Western blot results showed significantly increased expression of β-catenin and a significantly decreased expression of p-GSK3β in the Li-MBG scaffolds as compared to the MBG scaffolds without Li^+ on day 3 (Figure 3D). In conclusion, our results suggest that the Li-MBG scaffolds enhanced the activation of the Wnt/β-catenin pathway and subsequent osteogenic differentiation of BMSCs, as compared to the pure MBG scaffolds.

2.4. Efficacy of Li-MBG Scaffold for Cartilage Tissue Preservation

The efficacy of Li-MBG for osteochnodral defect repair were evaluated with histology of safranin-O staining. At 8 weeks after transplantation, the joint surface of the defect was filled with a little fibrous tissue and almost no neo-bone was formed in the non-treated group (**Figure 4**Aa,d). However, in the MBG group, the joint surface of the defect was filled with a mixture of fibrous and cartilage-like tissues, and neo-bone was found at the subchondral space (Figure 4Ab,e). Interestingly, in the Li-MBG group, a large amount of hyaline cartilage-like extracellular matrix at the surface as well as neo-bone at the subchondral space of the defects were observed (Figure 4Ac,f). The mean ICRS histological score also showed significant difference ($P < 0.05$) between the non-treated and MBG group. The score in the Li-MBG group was much higher than that of the MBG group ($P < 0.05$). After 16 weeks

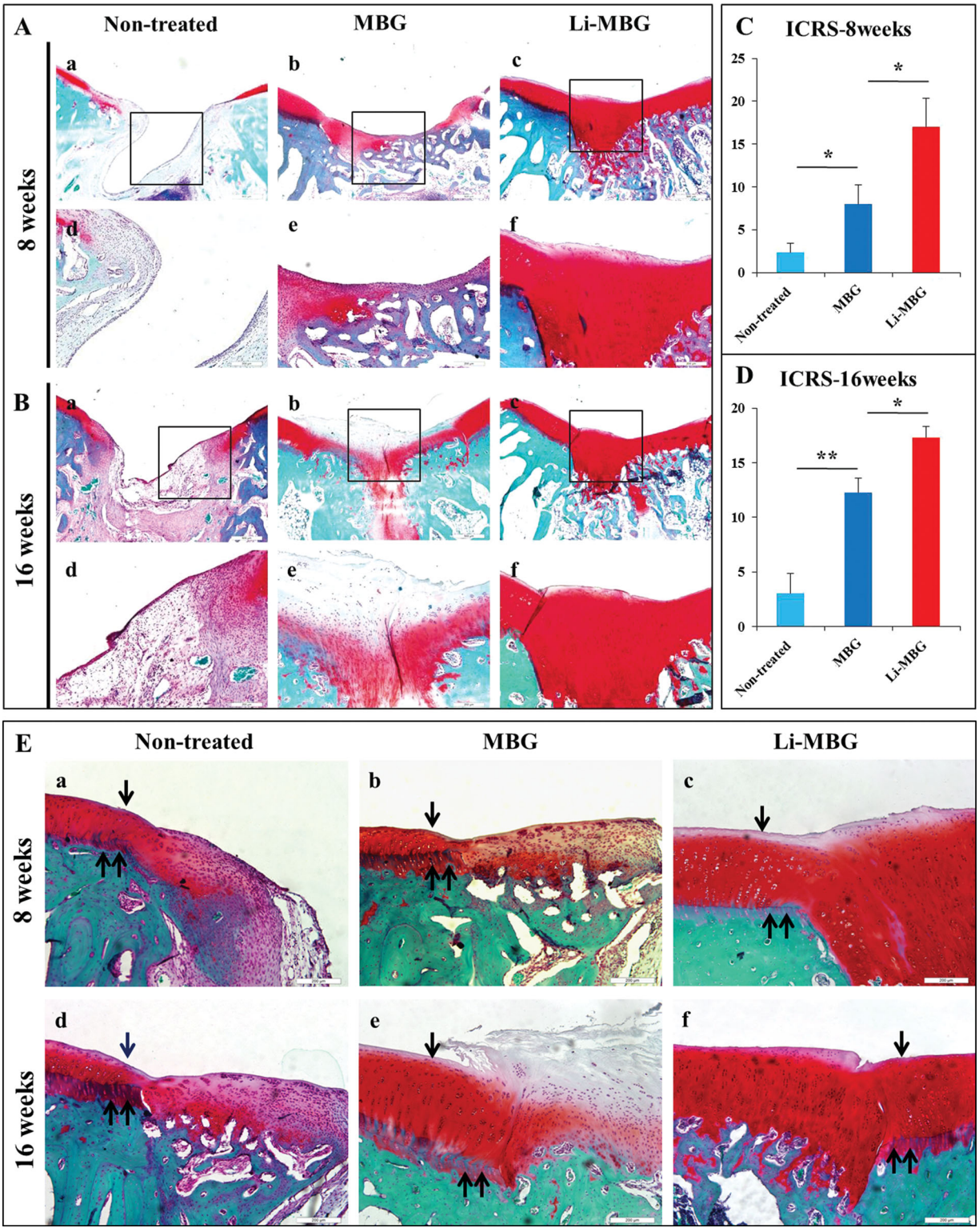

Figure 4. Histological evaluation at 8 and 16 weeks post-surgery. A) Histological sections from the three groups at 8 weeks. a,d) Non-treated group; b,e) MBG group, and c,f) Li-MBG group. B) Histological sections from the three groups at 16 weeks post-surgery. a,d) Non-treated group; b,e) MBG group and c,f) Li-MBG group. C) ICRS scoring on repaired cartilage at 8 weeks post-surgery. (D) ICRS scoring on repaired cartilage at 16 weeks post-surgery. Original magnification ×40; scale bar: 500 mm. (Ad–f) and (Bd–f): original magnification ×100; scale bar: 200 mm. A,B) Images of the bottom row represent the inset boxed area of the top row images at higher magnification. $*P < 0.05$, $**P < 0.01$. E) Histological sections from the three groups at 8 weeks (a–c) and 16 weeks (d–f) post-surgery. a,d) Non-treated group; b,e) MBG group and c,f) Li-MBG group. (Ea–f): original magnification ×100; scale bar: 200 mm. The edge of the defect is indicated with a black arrow. Tidemark is indicated with a double arrow.

of transplantation, the joint surface of the defect in the non-treated group was filled with more fibrous tissue compared to that at 8 weeks (Figure 4Ba,d), while the MBG group displayed a mixture of hyaline cartilage-like tissue and fibrous tissue (Figure 4Bb,e). Neo-bone could be found only in the MBG and Li-MBG groups but not in the untreated group. Bony tissue from the subchondral area almost bridged over the defect in both treated groups, but was denser in the Li-MBG group (Figure 4Bc,f). Interestingly, the Li-MBG group exhibited the greatest amount of hyaline cartilage-like tissue, which not only filled the surface but also displayed growth into the central part of the defect, thereby suggesting the stimulatory effect of Li^+ ions on cartilage preservation. In addition, ICRS histological score (Figure 4D) of the MBG group was approximately 2 times higher than that of the non-treated group ($P < 0.01$). The Li-MBG group exhibited the highest ICRS histological score among the three groups. These results thus suggest that the MBG scaffold incorporated with Li^+ ions is able to support both subchondral bone regeneration and cartilage formation.

In addition, the tidemark was observed at 8 and 16 weeks after transplantation, there was no tidemark detected in the defect in the non-treated group (Figure 4Ea,d). However, in the MBG group, the disordered connection structure was found between cartilage-like tissues and neo-bone (Figure [4]Eb,e). Interestingly, in the Li-MBG group, new tidemark formation was observed which was continuous with original tidemark (Figure 4Ec,f). These results thus suggest that the MBG scaffold incorporated with $Li^{\pm}$ ions is able to support stability repair of osteochondral defect.

2.5. Protective Effects of Li^+ ions on Cartilage Tissue Homeostasis In Vivo

To further investigate the mechanism of Li-MBG in cartilage tissue preservation, the protective effects of $Li^{\pm}$ ions alone on cartilage tissue was evaluated in C57Bl/6J mice OA model. Three days post-surgery, all mice were treated with either vehicle or LiCl daily by oral gavage for a total duration of 8 weeks before knee joints were harvested for analysis. Knee joints in the OA-vehicle group exhibited significant cartilage degeneration, with proteoglycan depletion and loss of surface lamina and fibrillations (**Figure 5**Ac). Li^+ ion treatment decreased the severity of these osteoarthritis-like changes (Figure 5Ad) by protecting cartilage from degradation and reducing the expression of two major proteinases—MMP13 and Adamts5 (Figure 5Ba–d). We did not observe any structural changes in the control knees in either vehicle or LiCl-treated mice (Figure 5Aa,b). Analysis of osteoarthritis pathology by the Osteoarthritis Research Society International (OARSI) scoring method indicated a significant decrease in the severity of osteoarthritis-like changes after LiCl treatment ($p < 0.05$), as compared with vehicle-treated mice (Figure 5Ae). These findings indicated that LiCl protects against cartilage ECM damage by reducing MMP13 and Adamts5 expression.

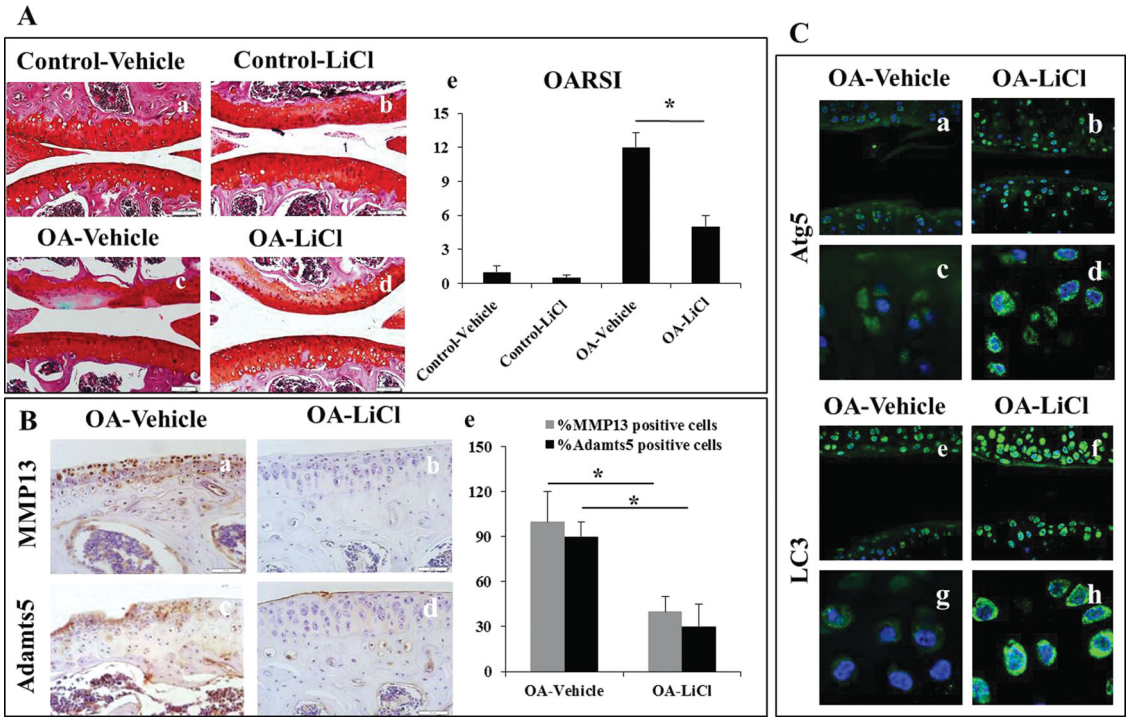

Figure 5. The inhibitory effect of Li^+ ions on OA progression upon systemic administration. A) Safranin O staining and OARSI scoring of knee joints after treatment. a) Control-vehicle group; b) Control-LiCl group; c) OA-vehicle group; d) OA-LiCl group; e) OARSI scoring of osteoarthritis severity. Magnification: ×20. Values are mean ± SD. *$p < 0.05$. B) Immunohistochemistry for detection of MMP13 and Adamts5 expression a) OA-Vehicle-MMP13, b) OA-LiCl-MMP13, c) OA-Vehicle-Adamts5, d) OA-LiCl-Adamts5, Magnification: ×40, e) Quantitative analysis of MMP13-positive and Adamts5-positive cells by measuring the ratio of MMP13 or Adamts5-positive cells to total cell number. *$p < 0.05$. C) Immunofluorescence staining for Atg5 and LC3. (a,c,e,g) OA-Vehicle, (b,d,f,h) OA-LiCl, (a,b,e,f). Original magnification: ×60, (c,d,g,h) Original magnification: ×180.

As Li was reported to play a protective role in neurodegenerative disease through activation of autophagy, we then set out to investigate whether the level of autophagy in cartilage was modulated by Li^+. Immunofluorescence analysis showed that the major autophagy markers—Atg5 and LC3, were expressed in a larger number of chondrocytes in LiCl-treated mice compared with vehicle-treated mice (Figure 5C). Based on these results, it is hypothesized that Li^+ ions may reduce MMP13 and Adamts5 expression through autophagy in vivo.

2.6. Underlying Mechanism of Cartilage Tissue Protection by the Li-MBG Scaffold

The underlying mechanisms involved in the protective effects of Li^+ ions was further investigated with chondrocyte culture model. Chondrocytes treated with IL-1β, an inflammatory factor which is widely used to induce OA-like changes in vitro, expressed much higher levels of MMP13 and Adamts5 (**Figure 6**Ca,b). Interestingly, activation of autophagy by LiCl reduced IL-1β levels and upregulated MMP13 and Adamts5 expression (Figure 6Cc,d), suggesting the protective effect of Li^+ ions on chondrocytes in vitro. Conversely, to inhibit autophagy, we utilized shRNA for Atg5, which is essential for autophagosome formation. RT-qPCR analysis showed a significant reduction of Atg5 mRNA ($p < 0.05$, Figure 6Aa). In addition, Western blot analysis showed that Atg5 protein was efficiently reduced by Atg5 shRNA compared with the control (Figure 6Ab). Additionally, the transfection of Atg5 shRNA significantly reduced the expression of LC3-II. These results thus indicated that Atg5 shRNA effectively reduced autophagy. Inhibition of autophagy by Atg5 shRNA-2 further enhanced IL-1β upregulation of MMP13 and Adamts5 expression (Figure 6Ca,b). The same trend was also observed in protein levels analyzed by Western blot (Figure 6B), indicating that LiCl ameliorated IL-1β-induced OA changes through autophagy, which explains the underlying mechanism in vivo.

3. Discussion

Li-MBG scaffolds were successfully fabricated, and were demonstrated to promote bi-lineage regeneration of osteochondral defects simultaneously through release of Li^+ ions. In our study, "bi-lineage" refers to two differentiated tissues (cartilage and bone) in vivo and two types of differentiated cells (osteoblasts differentiated from BMSCs and chondrocytes) in vitro. Li-MBG scaffolds could fulfill the requirements for regeneration of two types of tissues simultaneously within osteochondral defects in vivo. $Li^{\pm}$ ions released from Li-MBG enhanced the proliferation and osteogenic differentiation of BMSCs and protected chondrocytes respectively in vitro. The underlying

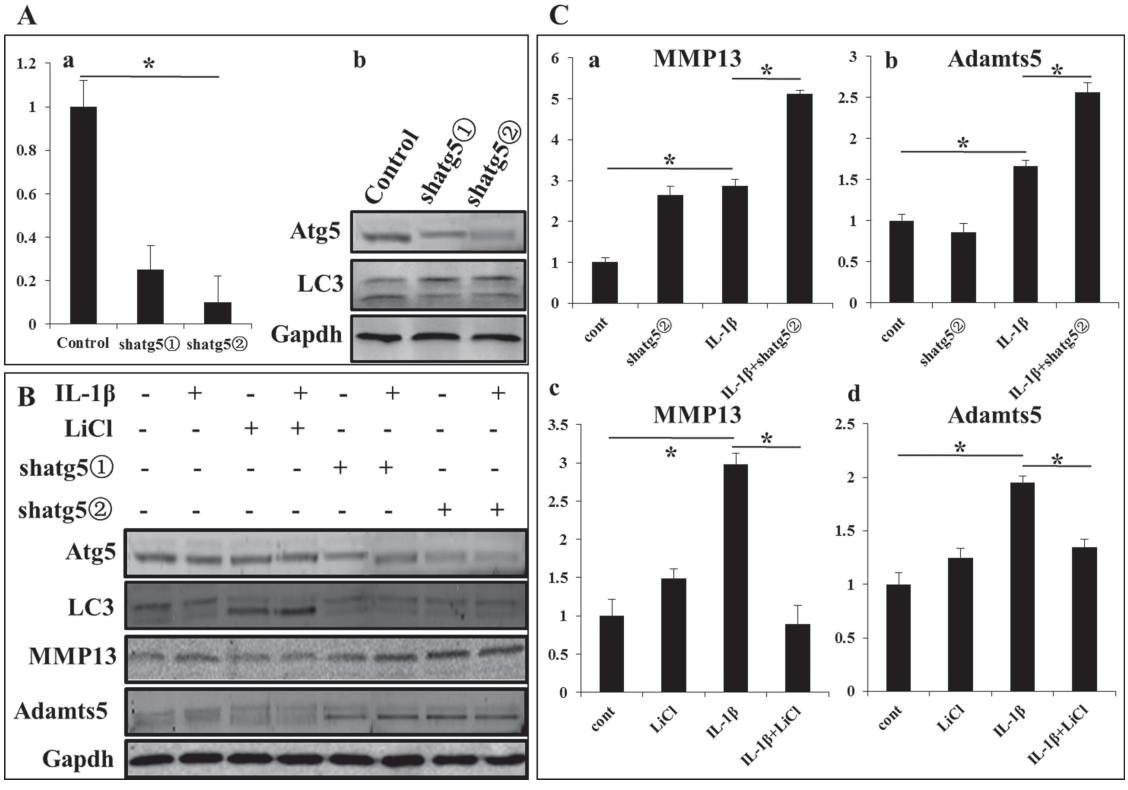

Figure 6. The effect of Li^+ ions on osteoarthritis-related gene expression in vitro. A) RT-qPCR for Atg5 mRNA (a) and Western blotting for Atg5 and LC3 (LC3,two migrating forms, LC3-I and LC3-II) protein (b) after transfection of control shRNA or ATG5 shRNA. B) Western blot analysis of Atg5, LC3, MMP13 and Adamts5 protein expression levels, after transfection of shRNA-1 or shRNA-2 for ATG5 or treatment with LiCl, with or without IL-1β stimulation. C) RT-qPCR for MMP13 and Adamts5 mRNA after transfection of shRNA-2 for Atg5 (a,b) or treatment with LiCl (c,d), with or without IL-1β stimulation. Values are mean ± SD. *$p < 0.05$.

mechanisms involve Li^+ ions protecting cartilage from degeneration via increased autophagy, as well as Li^+ ions promoting osteo-lineage differentiation of MSCs through activation of the Wnt signaling pathway.

In our study, it was shown that Li-MBG scaffolds can be utilized as a reliable platform for delivering Li^+ ions. The most interesting data is the ability of the Li-MBG scaffolds to promote the regeneration of bone and the preservation of hyaline cartilage-like tissues simultaneously. Previously, although various types of scaffolds have been developed for repair and regeneration of osteochondral defects, such as biphasic scaffold, multilayered scaffold and continuous non-stratified scaffold, these could not biologically mimic the natural structure and functional properties of cartilage and subchondral bone. Although various types of signaling molecules have been incorporated into scaffolds to enhance osteochondral defect regeneration, these often induced various adverse side effects. For example, some molecules that can protect cartilage from degeneration have the potential to trigger osteoarthritis through perturbation of subchondral bone homeostasis, that is, TGF-β signaling,[7,32] while some other molecules that can promote osteogenesis in subchondral bone may also increase chondrocyte calcification.[33] To our knowledge, there are few reports that utilized one scaffold type for regenerating both cartilage and subchondral bone simultaneously. In this study, Li^+ ions released from MBG scaffolds were found to promote subchondral bone regeneration, as well as protect against cartilage degeneration. These results thus suggest that the incorporation of Li^+ ions into MBG can be utilized as a bioactive scaffold for repair of osteochondral defects, which is beneficial to both bone regeneration and cartilage tissue preservation.

Subsequently, this study investigated the possible molecular mechanisms by which Li-MBG scaffolds preserved cartilage tissue. It was found that the released Li^+ ions protected cartilage tissue against degradation in an OA environment through increased autophagy. A previous study showed that autophagy played an important role in maintaining cartilage homeostasis and influenced the rate of articular cartilage degradation.[34] Li has been widely used as a long-term mood stabilizer for the treatment of bipolar and depressive disorders for half a century.[35,36] Recently, it was shown that Li plays a protective role in neurodegenerative disease by increasing the level of autophagy. This study found that Li^+ ions could protect against cartilage degradation through increased autophagy in a mouse osteoarthritis model. Additionally, we also observed that Li^+ ions could reverse the inhibition of autophagy and suppress the expression of OA-related genes such as MMP13 and Adamts5 induced by IL-1β. Hence, the sustained release of Li^+ ions led to a significant reduction in MMP13 and Adamts5 expression and osteoarthritis severity. Previous studies reported that the down-regulation of autophagy promoted OA-like gene expression in chondrocytes induced by inflammatory cytokines.[37] Rapamycin, a highly specific inhibitor of mTOR, can be utilized as a modulator of autophagy for OA treatment.[38] However, rapamycin has multiple pharmacological targets and also possess immunosuppressive properties, which could lead to severe adverse side effects. The clinical feasibility of using Li for the treatment of osteoarthritis is supported by recent studies utilizing Li instead of rapamycin for the treatment of neurodegenerative disease. Therefore, the mechanism of the observed stimulatory effect of Li-MBG scaffolds on cartilage preservation is related to the sustained release of Li^+ ions, which are demonstrated to protect cartilage tissue from degeneration via increased autophagy under OA conditions.

We further explored the possible molecular mechanisms by which Li-MBG scaffolds stimulated the regeneration of subchondral bone, and found that the released Li^+ ions enhanced the proliferation and osteogenic differentiation of BMSCs by activating the Wnt/β-catenin signaling pathway. Earlier studies have shown that Li^+ ions could enhance bone mass in vivo. However, there are as yet no reports that have investigated whether the released Li^+ ions from bioactive scaffolds exert effects on either the proliferation or osteogenic differentiation of BMSCs. Because previous studies showed that either too much or too little Li^+ ions inhibited cell proliferation and differentiation,[39,40] we went on to determine the appropriate concentration of Li^+ ions (5 mM) that can significantly enhance the growth and osteogenic differentiation of BMSCs. Hence, in this study, Li-MBG scaffolds were developed with this optimized concentration of Li^+ ions within the scaffolds. It was positively demonstrated that Li^+ ions released from the Li-MBG scaffolds significantly enhanced the proliferation and osteogenic gene expression (ALP, Runx2 and Ocn) levels of BMSCs. The Wnt family of signaling molecules has been reported to play a crucial role in BMSCs proliferation and osteo-lineage differentiation. Activation of Wnt signaling by either overexpression of β-catenin or through knock down of Wnt antagonists leads to denser and stronger bones in vivo.[41–44] These mechanistic studies illustrated that Li could inhibit GSK3β activity, thereby allowing β-catenin to accumulate in the cytoplasm for wnt pathway activation. These findings thus suggest that the sustained release of Li^+ ions from the Li-MBG scaffolds play a key role in promoting subchondral bone regeneration through activation of the Wnt/β-catenin signalling pathway.

4. Conclusions

Li-containing MBG scaffolds were fabricated, which enabled sustained release of Li^+ ions in situ. These exerted dual effects on both cartilage preservation and bone tissue regeneration. The Li-MBG scaffold successfully promoted renascence of subchondral bone and enhanced hyaline cartilage tissue restoration in rabbit models of osteochondral defects. The underlying mechanisms involve Li^+ ions enhancing the proliferation and osteogenic differentiation of BMSCs through activation of the Wnt signaling pathway, as well as Li^+ protecting chondrocytes and cartilage tissues from the inflammatory environment through up-regulating the level of autophagy. These findings thus suggest that Li-MBG is a bi-lineage conducive scaffold for osteochondral defect regeneration.

5. Experimental Section

Preparation of Scaffolds: Porous lithium-containing mesopore-bioglass (Li-MBG) scaffolds were prepared by incorporating Li (molar: 5%) into MBG, by using co-templates of nonionic block polymer P123 (EO20-PO70-EO20) and polyurethane sponges.[15] P123 is used to produce

mesoporous structures (mesopore size: several nanometers) and polyurethane sponges are used to create large pores (large pore size: several hundred micrometers). The prepared Li-MBG scaffolds have the chemical composition of Li, Ca, P, and Si with molar ratio of Li:Ca:P:Si at 5:10:5:80 (named Li-MBG). Pure MBG scaffolds (molar ratio Ca:P:Si = 15:5:80) were prepared by the same method and utilized as control materials. The effect of incorporation of Li into MBG on the dissolution of MBG was previously investigated. It was found that after incorporated parts of Li into MBG, more Si elements were released from scaffolds, indicating that Li ions may damage parts of the Si-O-Si tetrahedron structure and further improve the dissolution of MBG.[15]

Isolation and Culture of Cells: Bone marrow mesenchymal stem cells (BMSCs) were provided by Prof. He Huang.[45] Bone marrow cells were collected and then sifted with a cell sieve, seeded into a 25 cm^2 cell culture flask at a density of 2×10^6 cells mL^{-1}, and incubated in 5% CO_2 at 37 °C. The medium was initially changed 4 days after inoculation to remove the unattached cells, and then subsequently every three days until confluence was achieved. Continuous serial passage was performed in order to attain relatively pure BMSCs cultures. Cells between the 4th and 6th passages were treated as indicated in each experiment. Primary cultures of mouse chondrocytes and mouse articular cartilage were obtained from the femoral condyles and tibial plateaus of postnatal day 5–6 C57Bl/6 mice, as described previously.[46] Chondrocytes were maintained as a monolayer in DMEM supplemented with 10% fetal bovine serum at 37 °C. Cells between 0 to the 3rd passage were utilized for experiments.

Cell Proliferation Assay: The proliferation of BMSCs was assayed by the Cell Counting KIT-8 (CCK-8). The cells cultured on the scaffolds for 1, 3, 5, and 7 days in the growth medium, were incubated in 10% CCK-8 solution in a 5% CO_2 incubator at 37 °C for 3 h. The absorbance of the culture medium was measured at 450 nm. The cells were cultured in growth medium containing different concentrations of Li^+ ions (0, 2.5, 5, 10, and 15 mM), so as to investigate the effect of Li^+ ions on the proliferation of BMSCs. The detection method is described as above.

Ion Release From Li-MBG Scaffolds: To assay Li^+ ion release from the Li-MBG scaffolds, the spent medium was collected after culture at different time points. The ionic concentrations of Li^+ within the spent medium were determined by inductive coupled plasma atomic emission spectrometry (ICP-AES) (Perkin-Elmer Optima 7000DV).

Real-Time Polymerase Chain Reaction: The mRNA transcript levels of osteogenic specific genes (ALP, Runx2 and Ocn) and Wnt/β-catenin signaling specific genes (LEF-1, TCF-1 and Axin2) within BMSCs cultured on the scaffolds (1×10^5 cells per scaffold) in osteogenic-inducing medium were assessed by real-time PCR. All primer sequences (Invitrogen Inc., Carlsbad, CA, USA) were designed using the primer 5.0 software. Cells were harvested on day 3 and 7 and total cellular RNA was isolated by lysis in Trizol (Invitrogen Inc., Carlsbad, CA, USA). PCR was performed using SYBR Green QPCR Master Mix (Takara) with a Light Cycler apparatus (Bio-rad, CFX-Touch). The PCR cycling consisted of 40 cycles of amplification of the template DNA with primer annealing at 60 °C. The relative level of expression of each target gene was then calculated using the $2^{-\Delta\Delta}$Ct method. The amplification efficiencies of primer pairs were validated to enable quantitative comparison of gene expression. Each real-time PCR was performed on at least 3 different experimental samples and representative results are displayed as target gene expression normalized to the reference gene GAPDH. Error bars represent one SD from the mean of technical replicates. The following primer sequences were used: ALP sense 5′-CGGCCATCCTATATGGTAACGG-3′, antisense 5′-CAGGAG GCA TACGCCATCACA-3′; Runx2 sense 5′-CCAACTTCCTGTGCTCCGTG-3′, antisense 5′-GTGAAACTCTTGCCTCGTCCG-3′; Ocn sense 5′-GACCCTCTCTC TGCTCACTCT-3′, antisense 5′-GACCTTACTGCCCTC CTGCTTG-3′;TEF-1 sense 5′-CAAGCAGGTCTTCACCTCAGACA-3′, antisense 5′-CCGTGGTTACT GGGAGGAAGAG-3′; LEF-1 sense 5′-CAAATAAAGTGCCCGTGGTGC-3′, antisense 5′-CTGGACATGCCTTGTTTGGAGT-3′ and Axin2 sense 5′-TACCGG A GGATGCTGAAGGC-3′, antisense 5′-CCACTGGCCGATTCTTCCTT-3′. To analyze the expression levels of MMP13 and Adamts5, we examined the effects of inhibiting autophagy by shatg5 under stimulation with IL-1β in mouse chondrocytes. RT-PCR analysis was performed as described above. Mouse chondrocytes were pre-treated with 5 mM lithium 1 h prior to treatment with 10 ng mL^{-1} IL-1β. Twenty-four hours after treatment with IL-1β, RNA extraction was performed. Autophagy was suppressed by shRNA targeting ATG5. All shRNA were purchased from Invitrogen, for ATG5 no. 1, 5′-CCGGCCCGTGGAATGGAATGAGATTCTCGAGAATCTCA TTCCATTCCACGGGTTTTTG-3′; for ATG5 no. 2, 5′-CC G G C C G A C T T G T T C C T T A C G G A A A C T C G A G T T T C C G T A A GGAACAAGTCGGTTTTTG-3′; for Atg5, NC 5′-CCGGTTCTCCGAACGTGTC ACGTTTCAAG AGA A CGTGACACGTTCGGAGAATTTTTTG-3′. The following primer sequences were used: Atg5 sense 5′- TTGGAGTAGGTTTGGCTTTGGT-3′, antisense 5′- GGTTCT GCTTCCCTTTCAGTTATC-3′; MMP13 sense 5′-ATGCAGTCTTTCTTCGGC TT AG-3′, antisense 5′-ATGCCAT CGTGAAGTCTGGT-3′; Adamts-5 sense 5′-ATCAC –CCAATGCCAAGG-3′, antisense 5′-AGCAGAGTAGGAGACAAC-3′. The detection method is described as above.

Western Blot Analysis: To analyze the expression of GSK3β (Anbobio, AG751), pGSK3β-(Ser9) (Cell signaling, #9323) and β-catenin (Abcam, ab32527) at the protein level, Western blot analysis was performed. Briefly, after culturing BMSCs on scaffolds for 3 and 7 days, whole cellular protein was extracted with RIPA lysis buffer and the protein concentration was determined by the BCA Protein Assay Kit (Pierce #23227). The extracted protein was separated on SDS-PAGE gels. After electrophoresis, the protein was then transferred onto a polyvinylidene difluoride membrane and blocked in 5% non-fat milk for 4 h at room temperature. The membrane was incubated overnight at 4 °C with the antibody. After washing in Tris-buffered saline with Tween (TBST), horseradish peroxidase (HRP) conjugated secondary antibody was diluted 1:1500 in 5% bovine serum albumin (BSA) solution and then incubated with the membrane for 2 h at room temperature. Excess secondary antibody was rinsed off the membrane with TBST, and a chemiluminiscent signal was generated by using western blot detection reagents (ECL, Beyotime Institute of Biotechnology) according to the manufacturer's protocol. To determine the expression levels of Atg5 (Sigma, A0731), LC3 (Sigma, L7543), MMP13(Anbobio,C0263)and Adamts5 (Abcam, ab410370)at the protein level, we examined the effects of inhibiting autophagy by shatg5 under stimulation with IL-1β with mouse chondrocytes. Western blot analysis was performed as described above.

Alizarin Red Staining: BMSCs were seeded into 24-wells plate, and calcification was induced for 14 days with calcification medium. Lithium (5 mM) was added to the calcification medium during the induction of BMSCs to undergo calcium mineralization. Cultures of BMSCs were fixed with 4% (v/v) paraformaldehyde and then stained with alizarin red (0.5%). Specimens were visualized under a light microscope (X7; Olympus, Tokyo, Japan). For quantification of specimens, the cells were destained with 0.5 N HCl and 5% sodium dodecyl sulfate (SDS). Absorbance of the extracted dye was measured at 405 nm (TECAN).

Animal Model of Knee Joint Osteochondral Defect: All animals were treated according to standard guidelines approved by the Zhejiang University Ethics Committee. New Zealand white rabbits (2.5–3 kg) were maintained singly in stainless-steel cages. After general anesthesia, osteochondral cylindrical cartilage defects 4 mm in diameter and 5 mm deep were created on the patellar groove, on both the left and right limbs with a stainless-steel punch, which were then implanted with the scaffolds. The defects were untreated (Blank, $n = 8$ joints), or implanted with the MBG scaffold (n = 8 joints), or with the Li-MBG scaffold. After animal sacrifice, seven knee joints from each group were evaluated histologically at 8 and 16 weeks post-surgery.

Experimental Osteoarthritis in Mice: All mice were treated according to protocols approved by the Zhejiang University Ethics Committee. Experimental osteoarthritis was induced in 2-month-old male C57Bl/6J mice by transection of anterior cruciate ligament on the right knee. The left knee was not subjected to surgery and was used as a control. The animals were sacrificed 8 weeks after the knee surgery. Two independent experiments were performed. Each experiment included a total of 18 mice (nine mice treated with lithium chloride and nine mice receiving vehicle). Mice were fed chow containing 2 g of LiCl per kg of chow, for a duration of 10 weeks. Control mice were fed with LiCl-free chow under parallel conditions.

Gross Morphology and Safranin-O: At 8 and 16 weeks post-surgery, the rabbits were sacrificed by an intravenous overdose of pentobarbital. Seven samples from each group were examined and photographed for evaluation according to the International Cartilage Repair Society (ICRS) macroscopic assessment scale for cartilage repair.[47] After gross examination, seven paraffin sections from each sample were stained with safranin-O. The percentage of cartilage tissue in the area of the defect was calculated from the area that was stained positively for safranin-O. For the overall evaluation of regenerated tissue in the defects, the repaired tissues were graded blindly by three observers, using the ICRS Visual Histological Assessment Scale. At 10 weeks post-surgery, the mice were sacrificed. Paraffin sections from each sample were stained with safranin-O. The OARSI score of mice samples from each group were calculated.[48]

In Vivo Micro-CT Image Analysis: For micro-CT analysis, samples were first fixed with 4% paraformaldehyde for 48 h. Following image reconstruction, a constant region of interest with defects 4 mm in diameter and 5 mm deep was assigned. The reconstructed images were visualized and analyzed using Version 3. 1software provided by Shanghai Showbio Biotech Co., Ltd, SKYSCAN 1076). One sample was randomly selected from each group.

Immunohistochemistry and Immunofluorescence: Mice paraffin sections (6 μm) were incubated with 0.4% pepsin (Sangon Biotech, Shanghai, China) in 5 mM HCl at 37 °C for 20 min for antigen retrieval. Endogenous peroxidase was blocked by incubation with 3% hydrogen peroxide in methanol for 5 min. Non-specific protein binding was blocked by incubation with 2% BSA. After overnight incubation at 4 °C with primary antibodies, sections were then incubated with goat anti-mouse (Beyotime Institute of Biotechnology Inc., Jiangsu, China) secondary antibodies for 2 h at room temperature. The DAB substrate system (Zsbio, Beijing, China) was used for color development. Hematoxylin staining was used to reveal the cell nuclei. Mice specimens were fixed in 4% formalin solution for 20 min and 0.25% Triton X-100 in PBS for 15 min, and then incubated with primary antibody followed with goat anti-mouse secondary antibodies conjugated to Alexa Fluor 488 flourescent dyes (Invitrogen). Finally, cell nuclei were visualized by DAPI (Beyotime Institute of Biotechnology) and viewed under a confocal microscope system (Olympus, BX61W1- FV1000, Japan).

Acknowledgements

Funding for this study was provided by the National Key Scientific Research Projects (2012CB966604), Natural Science Foundation of China (81125014, J1103603 and 81101356), the National High Technology Research and Development Program of China (863 Program) (2012AA020503), Zhejiang Province Public Welfare Fund (2012C3112), The Recruitment Program of Global Young Talent, China (Dr. Wu), Shanghai Pujiang Talent Program (12PJ1409500), and the Natural Science Foundation of China (Grant 31370963, 81201202 and 81190132).

Received: December 29, 2013
Revised: February 12, 2014
Published online: April 22, 2014

[1] S. A. Oliveria, D. T. Felson, J. I. Reed, P. A. Cirillo, A. M. Walker, *Arthritis Rheum.* **1995**, *38*, 1134.
[2] J. Sellam, F. Berenbaum, *Nat. Rev. Rheumatol.* **2010**, *6*, 625.
[3] J. R. Steadman, W. I. Sterett, *Med. Sci. Sports Exerc.* **1995**, *27*, 328.
[4] M. Brittberg, A. Lindahl, A. Nilsson, C. Ohlsson, O. Isaksson, L. Peterson, *N. Engl. J. Med.* **1994**, *331*, 889.
[5] E. B. Hunziker, *Adv. Mater.* **2009**, *21*, 3419.
[6] D. B. Burr, M. A. Gallant, *Nat. Rev. Rheumatol.* **2012**, *8*, 665.
[7] G. Zhen, C. Wen, X. Jia, Y. Li, J. L. Crane, S. C. Mears, F. B. Askin, F. J. Frassica, W. Chang, J. Yao, J. A. Carrino, A. Cosgarea, D. Artemov, Q. Chen, Z. Zhao, X. Zhou, L. Riley, P. Sponseller, M. Wan, W. W. Lu, X. Cao, *Nat. Med.* **2013**, *19*, 704.
[8] Y. Tang, X. Wu, W. Lei, L. Pang, C. Wan, Z. Shi, L. Zhao, T. R. Nagy, X. Peng, J. Hu, X. Feng, W. Van Hul, M. Wan, X. Cao, *Nat. Med.* **2009**, *15*, 757.
[9] W. Fan, C. Wu, X. Miao, G. Liu, S. Saifzadeh, S. Sugiyama, I. Afara, R. Crawford, Y. Xiao, *J. Biomater. Appl.* **2013**, *27*, 979.
[10] M. Liu, X. Yu, F. Huang, S. Cen, G. Zhong, Z. Xiang, *Orthopedics* **2013**, *36*, 868.
[11] A. K. Lynn, S. M. Best, R. E. Cameron, B. A. Harley, I. V. Yannas, L. J. Gibson, W. Bonfield, *J. Biomed. Mater. Res. A* **2010**, *92*, 1057.
[12] J. Chen, H. Chen, P. Li, H. Diao, S. Zhu, L. Dong, R. Wang, T. Guo, J. Zhao, J. Zhang, *Biomaterials* **2011**, *32*, 4793.
[13] T. F. Day, X. Guo, L. Garrett-Beal, Y. Yang, *Dev. Cell* **2005**, *8*, 739.
[14] P. Clement-Lacroix, M. Ai, F. Morvan, S. Roman-Roman, B. Vayssiere, C. Belleville, K. Estrera, M. L. Warman, R. Baron, G. Rawadi, *Proc. Natl. Acad. Sci. U.S.A.* **2005**, *102*, 17406.
[15] P. Han, C. Wu, J. Chang, Y. Xiao, *Biomaterials* **2012**, *33*, 6370.
[16] F. Barry, M. Murphy, *Nat. Rev. Rheumatol.* **2013**, *9*, 584.
[17] S. Sarkar, R. A. Floto, Z. Berger, S. Imarisio, A. Cordenier, M. Pasco, L. J. Cook, D. C. Rubinsztein, *J. Cell. Biol.* **2005**, *170*, 1101.
[18] F. Fornai, P. Longone, M. Ferrucci, P. Lenzi, C. Isidoro, S. Ruggieri, A. Paparelli, *Autophagy* **2008**, *4*, 527.
[19] M. K. Lotz, B. Carames, *Nat. Rev. Rheumatol.* **2011**, *7*, 579.
[20] J. P. Pelletier, J. Martel-Pelletier, S. B. Abramson, *Arthritis Rheum.* **2001**, *44*, 1237.
[21] M. B. Goldring, M. Otero, *Curr. Opin. Rheumatol.* **2011**, *23*, 471.
[22] J. P. Pelletier, P. J. Roughley, J. A. DiBattista, R. McCollum, J. Martel-Pelletier, *Semin. Arthritis Rheum.* **1991**, *20*, 12.
[23] M. Kapoor, J. Martel-Pelletier, D. Lajeunesse, J. P. Pelletier, H. Fahmi, *Nat. Rev. Rheumatol.* **2011**, *7*, 33.
[24] J. R. Jones, L. M. Ehrenfried, L. L. Hench, *Biomaterials* **2006**, *27*, 964.
[25] Q. Z. Chen, I. D. Thompson, A. R. Boccaccini, *Biomaterials* **2006**, *27*, 2414.
[26] J. R. Jones, O. Tsigkou, E. E. Coates, M. M. Stevens, J. M. Polak, L. L. Hench, *Biomaterials* **2007**, *28*, 1653.
[27] X. Yan, X. Huang, C. Yu, H. Deng, Y. Wang, Z. Zhang, S. Qiao, G. Lu, D. Zhao, *Biomaterials* **2006**, *27*, 3396.
[28] X. Li, J. Shi, X. Dong, L. Zhang, H. Zeng, *J. Biomed. Mater. Res. A* **2008**, *84*, 84.
[29] C. Wu, Y. Zhang, Y. Zhou, W. Fan, Y. Xiao, *Acta Biomater* **2011**, *7*, 2229.
[30] C. Wu, Y. Zhang, Y. Zhu, T. Friis, Y. Xiao, *Biomaterials* **2010**, *31*, 3429.
[31] C. Wu, Y. Luo, G. Cuniberti, Y. Xiao, M. Gelinsky, *Acta Biomater.* **2011**, *7*, 2644.
[32] M. Wang, E. R. Sampson, H. Jin, J. Li, Q. H. Ke, H. J. Im, D. Chen, *Arthritis Res. Ther.* **2013**, *15*, R5.
[33] S. Zhu, P. Lu, H. Liu, P. Chen, Y. Wu, Y. Wang, H. Sun, X. Zhang, Q. Xia, B. C. Heng, Y. Zhou, H. W. Ouyang, *Ann. Rheum. Dis.* **2013**.
[34] B. Carames, N. Taniguchi, S. Otsuki, F. J. Blanco, M. Lotz, *Arthritis Rheum.* **2010**, *62*, 791.
[35] J. F. Cade, *Med. J. Aust.* **1949**, *2*, 349.
[36] J. Makoukji, M. Belle, D. Meffre, R. Stassart, J. Grenier, G. Shackleford, R. Fledrich, C. Fonte, J. Branchu, M. Goulard, C. de Waele, F. Charbonnier, M. W. Sereda, E. E. Baulieu, M. Schumacher, S. Bernard, C. Massaad, *Proc. Natl. Acad. Sci. U.S.A.* **2012**, *109*, 3973.
[37] H. Sasaki, K. Takayama, T. Matsushita, K. Ishida, S. Kubo, T. Matsumoto, N. Fujita, S. Oka, M. Kurosaka, R. Kuroda, *Arthritis Rheum.* **2012**, *64*, 1920.
[38] B. Carames, A. Hasegawa, N. Taniguchi, S. Miyaki, F. J. Blanco, M. Lotz, *Ann. Rheum. Dis.* **2012**, *71*, 575.
[39] C. A. Gregory, A. S. Perry, E. Reyes, A. Conley, W. G. Gunn, D. J. Prockop, *J. Biol. Chem.* **2005**, *280*, 2309.

[40] J. Cho, P. Rameshwar, J. Sadoshima, *J. Biol. Chem.* **2009**, *284*, 36647.
[41] T. F. Day, X. Guo, L. Garrett-Beal, Y. Yang, *Dev. Cell* **2005**, *8*, 739.
[42] F. Morvan, K. Boulukos, P. Clement-Lacroix, R. S. Roman, I. Suc-Royer, B. Vayssiere, P. Ammann, P. Martin, S. Pinho, P. Pognonec, P. Mollat, C. Niehrs, R. Baron, G. Rawadi, *J. Bone Miner. Res.* **2006**, *21*, 934.
[43] C. N. Bennett, K. A. Longo, W. S. Wright, L. J. Suva, T. F. Lane, K. D. Hankenson, O. A. MacDougald, *Proc. Natl. Acad. Sci. U.S.A.* **2005**, *102*, 3324.
[44] Z. Zhong, C. R. Zylstra-Diegel, C. A. Schumacher, J. J. Baker, A. C. Carpenter, S. Rao, W. Yao, M. Guan, J. A. Helms, N. E. Lane, R. A. Lang, B. O. Williams, *Proc. Natl. Acad. Sci. U.S.A.* **2012**, *109*, E2197.
[45] Y. Xu, L. Liu, L. Zhang, S. Fu, Y. Hu, Y. Wang, H. Fu, K. Wu, H. Xiao, S. Liu, X. Yu, W. Zheng, B. Feng, H. Huang, *PLoS One* **2012**, *7*, E34321.
[46] M. Gosset, F. Berenbaum, S. Thirion, C. Jacques, *Nat. Protoc.* **2008**, *3*, 1253.
[47] P. Mainil-Varlet, T. Aigner, M. Brittberg, P. Bullough, A. Hollander, E. Hunziker, R. Kandel, S. Nehrer, K. Pritzker, S. Roberts, E. Stauffer, *J. Bone Joint Surg. Am.* **2003**, *85-A* Suppl 2, 45.
[48] K. P. Pritzker, S. Gay, S. A. Jimenez, K. Ostergaard, J. P. Pelletier, P. A. Revell, D. Salter, W. B. van den Berg, *Osteoarthritis Cartilage* **2006**, *14*, 13.